Electromagnetic waves generated by ionospheric feedback instability

J. Y. Lu,[1,2] W. Wang,[3] R. Rankin,[1] R. Marchand,[1] J. Lei,[3] S. C. Solomon,[3] I. J. Rae,[1] J.-S. Wang,[2] and G.-M. Le[2]

Received 18 July 2007; revised 7 January 2008; accepted 29 January 2008; published 6 May 2008.

[1] A new interactive M-I coupling model that describes the dynamic interaction between magnetospheric dispersive waves, compressional modes, and auroral electron precipitations is applied to investigate the geomagnetic electromagnetic pulsations observed in Earth's magnetosphere in terms of magnetospheric waves triggered by ionospheric feedback instability. Two new aspects of this work are that (1) we treat the full nonlinear MHD equations, i.e., include the full compressional modes and their coupling with shear Alfvén waves in the magnetosphere; and (2) the height-integrated Pedersen conductivity is treated as a dynamic parameter by electrodynamically coupling the 2D finite element wave model "TOPO" to the ionospheric ionization model "GLOW". It is shown that the feedback instability can be triggered by a very small-scale, small amplitude density perturbation; and the small-scale electromagnetic oscillations and their associated density fluctuations observed in magnetosphere can be attributed to the feedback instability. We demonstrate that, unlike in a field line resonance where the ponderomotive force causes the plasma to move mainly along the field line, the plasma in the feedback instability is distributed either as a bump or a cavity along a field line and leads to a multibanded structure in the radial direction. The nonlinear feedback instability model can successfully explain the formation of plasma density and electromagnetic perturbations with the same frequency, which disagree with current FLR scenario.

Citation: Lu, J. Y., W. Wang, R. Rankin, R. Marchand, J. Lei, S. C. Solomon, I. J. Rae, J.-S. Wang, and G.-M. Le (2008), Electromagnetic waves generated by ionospheric feedback instability, *J. Geophys. Res.*, *113*, A05206, doi:10.1029/2007JA012659.

1. Introduction

[2] In the magnetosphere-ionosphere coupling, the ionosphere is usually treated as a passive screen upon which the patterns of magnetospheric activity are drawn, and the magnetosphere plays the most important role in most of the auroral dynamics [*Lysak*, 1990]. However, since the ionospheric current system in the auroral zone is connected with the magnetospheric current system via field-aligned currents, the ionosphere can also be an initiator of aurora formation, even though disturbances initiating aurora from the ionosphere may not be as dramatic as those processes driving aurora from the magnetosphere [e.g., *Atkinson*, 1970; *Watanabe et al.*, 1993]. The ionospheric feedback instability caused by temporal variations of ionospheric conductivity represents a type of processes in which the ionosphere plays the role of a generator which drives auroral dynamics [e.g., *Atkinson*, 1970; *Sato*, 1978; *Miura and Sato*, 1980]. The driver of the ionospheric feedback instability is the convection electric field and the changes in the ionospheric conductivity (or density) can be produced either by precipitating electrons in upward field-aligned current regions or by artificial rf heating experiments in the E-region ionosphere. If a convection electric field exists, the density/conductivity enhancement can induce a polarized electric field whose direction is oppose to the original convection electric field, and the requirement of current continuity then produces secondary field-aligned currents associated with the emission of an upward propagating Alfvén wave into the magnetosphere; when this Alfvén wave is reflected back toward the ionosphere, either at the conjugate ionosphere or at regions of large gradients in the Alfvén speed, a positive feedback can result if the phase of the reflected wave is such that the electrons associated with upward field-aligned current of this wave impact the ionosphere at the previously established conductivity enhancement, increasing the conductivity further [*Miura and Sato*, 1980].

[3] The ionospheric feedback instability has been invoked as a possible explanation for small-scale auroral arcs [*Atkinson*, 1970; *Holzer and Sato*, 1973; *Sato*, 1978; *Lysak and Song*, 2002; *Pokhotelov et al.*, 2002b; *Streltsov et al.*, 2005]. While many features of some auroral arcs, such as the periodic intensification, FACs, electric fields, and den-

[1]Department of Physics, University of Alberta, Edmonton, Alberta, Canada.
[2]National Center for Space Weather, China Meteorology Administration, Beijing, China.
[3]High Altitude Observatory, National Center for Atmospheric Research, Boulder, Colorado, USA.

0148-0227/08/2007JA012659

sity cavities, can be attributed to shear Alfvén wavefield line resonances (FLRs) as an externally driven phenomenon [e.g., *Rankin et al.*, 2005; *Lu et al.*, 2003b, 2007], the long oscillation period complicates interpretations of the in situ data. The importance of the Ionospheric Alfvén Resonator (IAR) for small-scale arcs formation was also suggested and the excitation of the IAR is usually attributed to a feedback instability [*Trakhtengertz and Feldstein*, 1984, 1991; *Lysak*, 1991; *Mishin and Banaszkiewicz*, 1998; *Pokhotelov et al.*, 2003]. Ionospheric feedback instability develops much quicker to reach the very small spacial scale structures observed in auroral arcs. Observations show that discrete auroral arcs (the visible features usually at 1–100 km scales) usually have multibanded structures and more frequently occur at nighttime, in the winter, and at solar minimum [*Newell et al.*, 1996, 1998; *Liou et al.*, 1997, 2001]. These observations suggest that either the lower conductivity under dark conditions enhances aurora, or the plasma density in the auroral acceleration region is lower under such conditions. On the other hand, theoretical and numerical studies of the ionospheric feedback mechanism by *Trakhtengertz and Feldstein* [1991], *Lysak and Song* [2002], *Streltsov and Lotko* [2004], and *Streltsov et al.* [2005] demonstrate that the instability develops when the background ionospheric conductivity is low. Also, low densities in the acceleration region will enhance parallel electric fields [*Song and Lysak*, 2001; *Tikhonchuk and Rankin*, 2002]. All these studies suggest that the ionospheric feedback mechanism may be an important mechanism for the formation of narrow auroral arcs. *Lysak and Song* [2002] calculated the Pedersen conductivity modulations resulting from ionospheric over-reflection of Alfvén wave energy. *Streltsov and Foster* [2004] considered electrons precipitating through parallel currents, finding that the dependency of the Pedersen conductivity on the parallel current can lead to the ionospheric feedback instability within the Alfvénic resonator. Some other investigations also confirmed that the ionospheric feedback instability plays an important role in the formation of small-scale auroral arcs [e.g., *Lysak*, 1991; *Pokhotelov et al.*, 2002a, 2002b; *Streltsov et al.*, 2005].

[4] Recently the ionospheric feedback instability has received renewed attention in explaining the geomagnetic ultra-low-frequency (ULF) pulsations [e.g., *Streltsov and Mishin*, 2003; *Streltsov and Foster*, 2004; *Streltsov and Lotko*, 2004; *Streltsov et al.*, 2005]. ULF oscillations are not only frequently observed in the auroral zone, but also at sub-auroral latitudes where no measurable electron precipitation was present [*Mishin et al.*, 2003]. *Streltsov and Mishin* [2003] modeled the small-scale wave structures observed by DMSP satellite in the sub-auroral zone in terms of Alfvén waves generated by the ionospheric feedback instability. They demonstrated that a small-scale density fluctuation on the ionospheric bottom can trigger the development of instability. In another study, *Streltsov et al.* [2005] investigated the generation of small-scale FACs by the ionospheric feedback instability triggered by the HF heating of the ionosphere and confirmed again that the instability develops when the conductivity in both ionospheres is low. In all these studies, the ULF pulsations are interpreted as shear Alfvén waves (SAWs) as a consequence of the development of ionospheric feedback instability.

[5] However, previous studies so far either have no auroral electron precipitation [e.g., *Pokhotelov et al.*, 2002a; *Streltsov and Lotko*, 2004; *Streltsov et al.*, 2005] or use a simplified electron source term [e.g., *Atkinson*, 1970; *Holzer and Sato*, 1973; *Sato*, 1978; *Miura and Sato*, 1980; *Lysak*, 1991; *Lysak and Song*, 2002]. *Watanabe et al.* [1993] first introduced the parallel anomalous resistivity to generate the field-aligned potential drop. They used the Fridman-Lemaire formula to estimate the FACs from auroral electron precipitation and a simple fitting function to calculate the ionization rate from potential drop [*Watanabe et al.*, 1993, equation (12), (14)]. This precipitation model was adopted by *Pokhotelov et al.* [2002b] who includes the contribution of finite electron inertia and temperature in a non-uniform magnetospheric model.

[6] Also, no efforts have been made to analyze the interaction between SAW and compressional modes in dispersive scale. Radar and satellite observations in the auroral and sub-auroral zones demonstrate that there exist the extended field-aligned density cavities associated with localized electromagnetic waves and that the density profile inside the cavity is highly variable [e.g., *Persoon et al.*, 1988; *Doe et al.*, 1993; *Mishin et al.*, 2003; *Chaston et al.*, 2006]. Theory and computations of FLRs have shown that the nonlinear ponderomotive force leads to the density redistribution along the magnetic field lines, resulting in localized density cavities which may trap the shear Alfvén waves [*Lu et al.*, 2003b]. Such density redistribution in the magnetosphere can steepen the local Alfvén speed gradient and then significantly affects the dynamic evolution of a standing shear Alfvén wave [*Lu et al.*, 2003a, 2003b]. However, the FLR scenario has difficulty in explaining some small-scale arcs with long oscillation period and also disagree with the observed subauroral wave structure from DMSP satellite [*Mishin et al.*, 2003; *Mishin and Burke*, 2005].

[7] These previous work have clearly demonstrated the importance of the ionosphere feedback instability on auroral dynamics and advanced our understanding of the role of Alfvén waves in the M-I coupling. However, these studies used a linear magnetosphere model and very simple ionospheric conductance models that do not take into full account the active response of the ionosphere to auroral precipitation inputs. In this paper, we make a full MHD magnetospheric calculation of the dispersive SAWs in dipolar geometry, and an ionospheric model (the GLOW model) that self-consistently calculate ionospheric ionization rates produced by auroral precipitation. The improved ionospheric conductivity model considers the effects of field-aligned potential drops and magnetic mirror, and calculate the mean energy from FACs using the Knight-relationship [*Knight*, 1973; *Wiltberger et al.*, 2004]. We investigate the development of Alfvén waves triggered by ionospheric feedback instability and their coupling with compressional modes. We explain the density perturbations associated with the geomagnetic pulsations frequently observed in the auroral and sub-auroral magnetosphere.

2. Model of the Active Auroral Ionosphere

[8] FACs play an important role in magnetosphere-ionosphere coupling. In particular, magnetospheric field-

aligned currents are closed by field-crossing ionospheric currents. Here, we shall neglect the ionospheric Hall current for simplicity, and write the current continuity equation as

$$\nabla_\perp \cdot (\Sigma_P \mathbf{E}_\perp) = -j_\parallel \tag{1}$$

where Σ_p is the ionospheric height-integrated Pedersen conductivity; the subscripts $\perp$ and $\parallel$ denote vector components in the directions perpendicular or parallel to the magnetic field, respectively. The variation of ionospheric conductivities leads to a feedback effect on the magnetospheric FACs.

[9] The ionization in the ionospheric E-layer is produced mainly by electron precipitation and solar radiation. The electron density continuity equation in the E-layer can be simplified as [*Sato*, 1978]

$$\frac{\partial n}{\partial t} = -R\left(n^2 - n_0^2\right) - \frac{j_\parallel}{eh} + \gamma_{\text{hot}}, \tag{2}$$

where n_0 is the background electron density produced by solar illumination (in the absence of the field-aligned current); $R \approx 3 \times 10^{-7}$ cm^3/s is the constant of recombination [*Nygrén et al.*, 1992], and γ_{hot} is the ionization rate due to auroral (hot) electron precipitation. In this paper we shall focus on the wave dynamics in the nighttime, thus all ionizations are produced by auroral electron precipitation.

[10] To calculate the ionospheric E region ionization rate produced by particle precipitation, we relate FACs to the characteristic energy (or average energy) and energy flux of particle precipitation. Then, we use these parameters as inputs to a thermosphere-ionosphere model, GLOW, to obtain the ionization rate. Detailed procedure can be found by *Lu et al.* [2007]. It should be noted that GLOW is a physics based model that is able to describe the dynamical response of the ionosphere to changes in particle precipitation that are related to both spatial and temporal variations of field aligned currents and magnetospheric conditions [*Solomon et al.*, 1988; *Solomon and Abreu*, 1989]. The GLOW model thus allows us to simulate spatial (latitude and longitude as inputs) and temporal (universal time as input) response of the upper atmosphere to auroral inputs.

[11] We note in passing that two studies of ionospheric feedback instability by *Watanabe et al.* [1993] and *Pokhotelov et al.* [2002b] used the non-linear generalization of the Knight relationship by *Fridman and Lemaire* [1980] to estimate FACs by auroral electron precipitation, but the non-physics based empirical formula by *Banks et al.* [1974] to obtain the ionization rate from the field-aligned potential drop. As pointed out by *Pokhotelov et al.* [2002a], from a theoretical point of view, a kinetic treatment of auroral electrons [e.g., *Rankin et al.*, 1999] would be more appropriate than the simplified model of auroral electron precipitation described above. The kinetic model, however, is much harder to implement numerically. Fortunately, for the numerical solution discussed in this paper, the field-aligned current carried by auroral electrons does not exceed 15% of the total field-aligned current; we therefore can reasonably neglect the kinetic contribution of the hot electrons to the MHD field-aligned current in equation (2) avoiding complications of the kinetic approach.

3. MHD Model of the Magnetosphere

[12] The nonlinear interaction of shear Alfvén FLRs and compressional modes in the warm inhomogeneous magnetospheric plasma is governed by the MHD equations

$$\frac{\partial \mathbf{B}}{\partial t} = -\nabla \times \mathbf{E}, \qquad \mu_0\left(\mathbf{j} + \varepsilon_0 \frac{\partial \mathbf{E}_\perp}{\partial t}\right) = \nabla \times \mathbf{B}; \tag{3}$$

$$\mathbf{E} = -(\mathbf{v} \times \mathbf{B}) - \frac{\nabla P_e}{ne} + \frac{m_e}{ne^2}\frac{\partial \mathbf{j}}{\partial t}; \tag{4}$$

$$\frac{\partial \rho}{\partial t} + \rho \nabla \cdot \mathbf{v} + \nabla \rho \cdot \mathbf{v} = 0; \tag{5}$$

$$\rho \frac{\partial \mathbf{v}}{\partial t} + \rho \mathbf{v} \cdot \nabla \mathbf{v} = -\nabla P + \mathbf{j} \times \mathbf{B}; \tag{6}$$

$$\frac{\partial P}{\partial t} + \gamma P \nabla \cdot \mathbf{v} + \mathbf{v} \cdot \nabla P = 0; \tag{7}$$

Where P_e and m_e are the thermal pressure and mass for electron (e) only.

[13] Note that the above equations are not linearized MHD equations. The full wave nonlinearities, including its coupling with compressional modes, are accounted for. This is especially important when the plasma sheet is hot and the magnetic field is weak, as in the nighttime magnetosphere. *Lu et al.* [2007] demonstrated that in high-β situations, where reduced MHD breaks down, new behavior can occur due to high plasma pressure effects and nonlinearized MHD solutions are required. Also, the perpendicular component of the displacement current is included in equation (3). The inclusion of this term becomes important in regions where the Alfvén velocity approaches the light speed. According to a recent study [*Song and Lysak*, 2001], the displacement current is possibly essential to the evolution of parallel electric fields and the establishment of FAC in certain situations. In the generalized Ohm's law, we include the pressure gradient and electron inertia because the dynamics of SAWs may be strongly affected by these dispersive processes [*Lu et al.*, 2003a, 2003b]; and we neglect the Hall term since it is important only when the frequency approaches the ion gyrofrequency, i.e., for frequencies much higher than are considered in this paper.

4. Numerical Results

[14] Electron precipitation is associated with field-aligned static or quasi-static potential drops, therefore related to the total parallel current. In the context of waves, the FAC and its characteristic width is associated with the perpendicular scale of shear Alfvén waves formed in the magnetosphere. A self-consistent study therefore requires solving both the set of equations for the magnetospheric SAWs and the

equations given in section 2 for auroral electron precipitations. Here, we combine the GLOW model for auroral electron precipitation with the magnetospheric wave model TOPO described by *Lu et al.* [2003b], which describes the excitation of parallel currents and electric fields in the wavefields of field line resonances. The finite element model TOPO [*Marchand and Simard*, 1997] is used to solve the 2D MHD equations (9)–(13) for magnetospheric waves [*Lu et al.*, 2003b] and 1D equations (1) and (2) for ionospheric electrons. The model for magnetospheric waves takes into account the full compressional modes and the variation of temperature and density along and across the magnetic field lines, together with wave dispersive effects which become important when the perpendicular scale of SAWs approaches the electron inertial scale at the ionosphere [*Hasegawa and Wakatani*, 1983; *Frycz et al.*, 1998; *Lu et al.*, 2003b].

[15] The background magnetospheric parameters are similar to those given by *Streltsov et al.* [2005]: The density inside the computation domain is modeled as $n_0 = n_{01}n_{02}$, and

$$n_{01} = 2 - \cos\left[(L - 7.5) * \pi\right] \tag{8}$$

$$n_{02} = \begin{cases} a_1(r - r_1) + a_2 & \text{if } r_1 < r < r_2 \\ b_1 e^{-20(r-r_2)} + b_2 r^{-4} + b_3 & \text{if } r > r_2 \end{cases} \tag{9}$$

Here L is the dipole magnetic shells, r is the radial distance in Earth radii to the point on $L = 7.5$, $r_1 = 1 + 120/R_e$(E-Layer maximum), $r_2 = 1 + 320/R_e$(F-layer maximum), and the constants a_1, a_2, b_1, b_2, and b_3 are chosen to provide plasma density of 3×10^4 cm^{-3} at the altitude 120 km, 3×10^5 cm^{-3} at the altitude 320 km, and 0.5 cm^{-3} at the equatorial magnetosphere. Along a given magnetic field line, the initial background electron and ion temperatures (T_{e0} and T_{i0}) are chosen to satisfy the equilibrium condition of constant pressure from $\mathbf{B_0} \cdot \nabla(n_0 T_{e0,i0}) = 0$, using initial electron and ion temperatures for $L = 7.5$ at the equator, $T^{eq}_{e0,i0}$, respectively.

[16] We consider a current-free equilibrium state for the initial condition. As done in many previous studies [e.g., *Streltsov and Mishin*, 2003; *Streltsov et al.*, 2005], the initial convection electric field $E_\perp 0$ in the ionosphere is chosen to be inversely proportional to n_0 so that $\nabla_\perp \cdot (\Sigma_{p0} E_{\perp 0}) = 0$. Inside the computational domain between $L = 6.5$ to $L = 8.5$, $E_{\perp 0}$ is defined by projecting it equipotentially along dipole magnetic field lines connecting the northern and southern ionospheres. In our calculation, the maximum values of the initial convection electric field is 40 mV/m in the ionosphere. Since the physical processes mainly occur in the ionospheric regions and around shell $L = 7.5$ during our calculation time, Non-linear meshes are used in both along and across the magnetic field lines to reduce the calculation time. To capture the small-scale feature of the instability, our maximum resolutions are 60 km in the direction along the field lines, and 42 km in the direction across the L shell at the equator.

[17] We drive the shear Alfvén waves and compressional modes by an initial small amplitude (1%) density perturbation only at the northern ionosphere. This ionospheric density disturbance will cause the fluctuation of the ionospheric conductivity, which according to equation (1) generates field-aligned currents flowing from the ionosphere to the magnetosphere, just as demonstrated in previous studies [e.g., *Drozdenko and Morales*, 2000; *Streltsov and Mishin*, 2003; *Streltsov and Lotko*, 2004; *Streltsov et al.*, 2005].

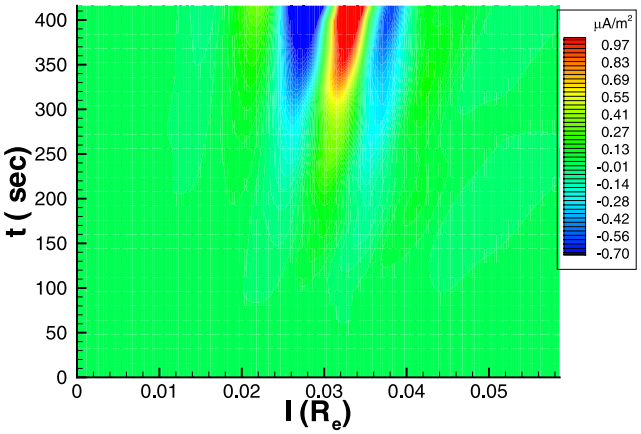

Figure 1. Temporal development of parallel currents at the southern ionosphere triggered by a small amplitude density perturbation in the northern ionosphere. l corresponds to the distance in Earth radii from the inner boundary across field lines.

[18] Figure 1 shows the temporal development of the FAC at southern ionosphere for $T^{eq}_{e0} = 400$ eV and $T^{eq}_{i0} = 1000$ eV. Although only a very small amplitude perturbation is exerted only on northern ionosphere boundary, the shear Alfvén wave is excited and propagates in magnetosphere along the field line between conjugate ionospheres. At $t = 400$ s, the parallel current increases to over 1 μA/m^2 from zero initially. In this computation, the minimum initial plasma density in the E-region of both ionospheres is 3×10^4 cm^{-3}, corresponding to a minimum Σ_{p0} of 1 mho. This agrees well with the results of other studies [e.g., *Drozdenko and Morales*, 2000; *Streltsov and Lotko*, 2004] that the instability can develop when the ambient ionospheric conductivity is low. The wave structure exhibits a band structure across the field lines.

[19] To see the effects of auroral electron precipitation, we compare the wavefields with and without auroral electron precipitation by including/excluding the auroral ionization rate term in equation (2), respectively. Figure 2 gives the wavefields across the magnetic field at the southern ionosphere at $t = 400$ s, dashed line representing the case with auroral electron precipitation, while solid line without the contribution from electron precipitation. The precipitating electrons cause an enhancement in the Pedersen conductivity, and all the wavefields get significant increases in comparison to the case without precipitating electrons: the amplitude of the azimuthal magnetic field is enhanced from 10 nT to 60 nT, the field-aligned current from 0.2 to 1.8 μA/m^2, and the perpendicular electric field from 15 mV/m to 155 mV/m.

[20] In Figure 3, we present the wavefields at the southern ionosphere for the cases with different precipitation energies at $t = 400$ s, respectively. We calculate three cases: (1) $T^{eq}_{e0} = 100$ eV, $T^{eq}_{i0} = 200$ eV (dashed); (2) $T^{eq}_{e0} = 200$ eV, $T^{eq}_{i0} = 400$ eV (dotted); and (3) $T^{eq}_{e0} = 400$ eV, $T^{eq}_{i0} = 1000$ eV (solid).

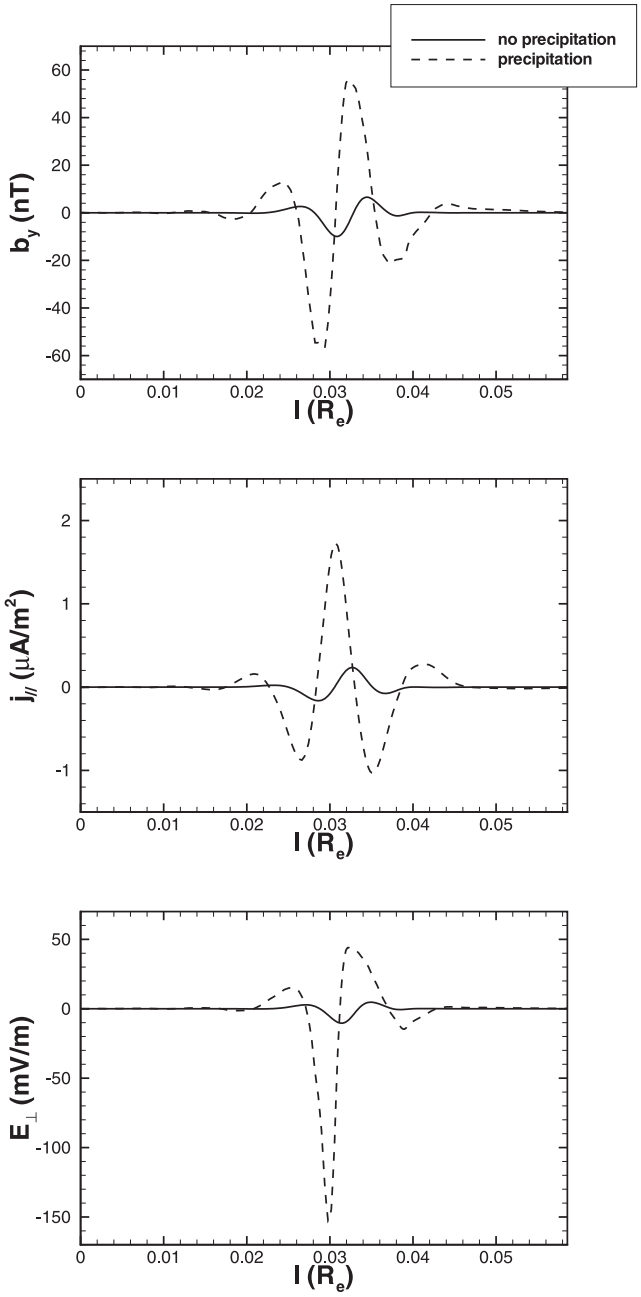

Figure 2. Radial dependence of azimuthal magnetic field b_y, parallel current $j_{\|}$, and perpendicular electric field $E_\perp$ at the southern ionosphere triggered by a small amplitude density perturbation in the northern ionosphere at $t = 400$ s. The solid line does not have contributions from auroral electron precipitation; the dashed line corresponds to a case with precipitating energy 1.8 keV. l corresponds to the distance in Earth radii from the inner boundary across field lines.

For 1 μA/m^2, the corresponding characteristic precipitation energies at $t = 400$ sare 625 eV, 975 eV, and 1.8 keV and energy fluxes are 0.05, 0.09, and 0.22 g cm^3 s^{-3}, respectively. It can be seen that a larger field-aligned current and stronger particle precipitation (higher mean energy and larger number flux) are observed when the initial magnetospheric plasma temperatures are higher, that is, the feedback instability grows much faster for the higher precipitating energy and energy flux. However, at the stage of lower amplitude FACs, auroral precipitating electrons has no significant effect in feeding back the magnetospheric waves.

[21] The nonlinear ponderomotive force in the wavefield leads to density redistribution along the magnetic field lines. Figures 4 and 5 show the compressional waves v_x and v_z at $t = 400$ s, respectively. v_x and v_z are roughly 10–50 times smaller than the azimuthal movement (max-

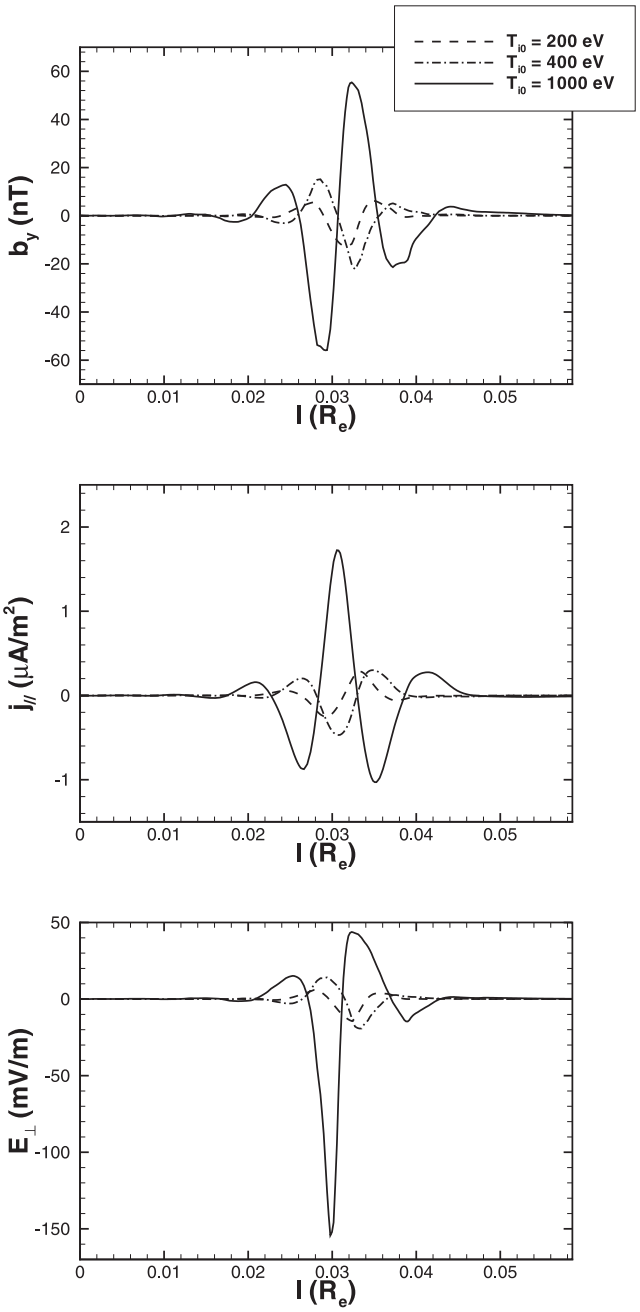

Figure 3. Radial dependence of azimuthal magnetic field b_y, parallel current $j_{\|}$, and perpendicular electric field $E_\perp$ at the southern ionosphere for three different precipitating energies (discussed in the text), respectively. l corresponds to the distance in Earth radii from the inner boundary across field lines.

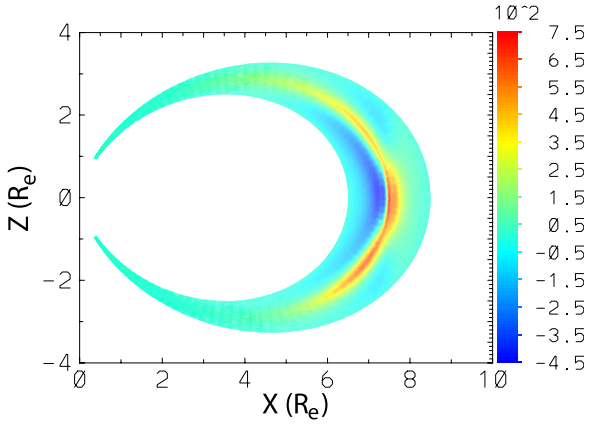

Figure 4. Compressional component v_x due to ponderomotive force at $t = 400$ s for the instability case in Figure 1.

imum $v_y \sim 3 \times 10^4$ m/s at this time). The plasma movements are very different from that associated with FLRs: for example, across the field lines at the equatorial plane, there is plasma moving earthward (in blue) and anti-earthward (in red); while in FLR, the plasma moves along the field line from high to low latitude [*Rankin et al.*, 1999; *Lu et al.*, 2003b]. As a result, density redistributions are different in FLRs and in the instabilities, as shown in Figure 6 for the relative density perturbation $\delta\rho/\rho_0$. In FLR, the plasma mainly moves along the field lines, especially on the resonance shell, resulting in density bump at the equator and cavity in the high latitudes close to the ionosphere; density and wavefield oscillations have different frequency across the magnetic field lines, as shown in Figure 6b [also see *Lu et al.*, 2003b]. While in the feedback instabilities in Figure 6a, density is distributed either as bump or cavity along the field line, and across the field lines, cavity and bump occur alternately; the plasma density and electromagnetic variations have the same frequency. For the similar amplitudes of wavefields, such as parallel currents, azimuthal magnetic field, and perpendicular electric field, the maximum density perturbation associated with the instability is smaller than those generated from FLRs. It can be deduced that the very large scale and large amplitude cavity across the field line is more likely generated by FLRs.

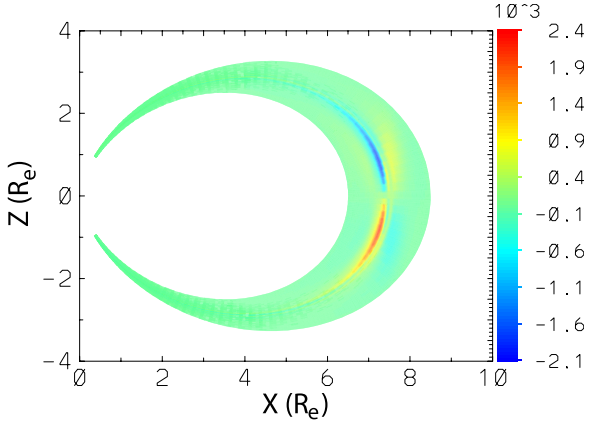

Figure 5. Compressional component v_z due to ponderomotive force at $t = 400$ s for the instability case in Figure 1.

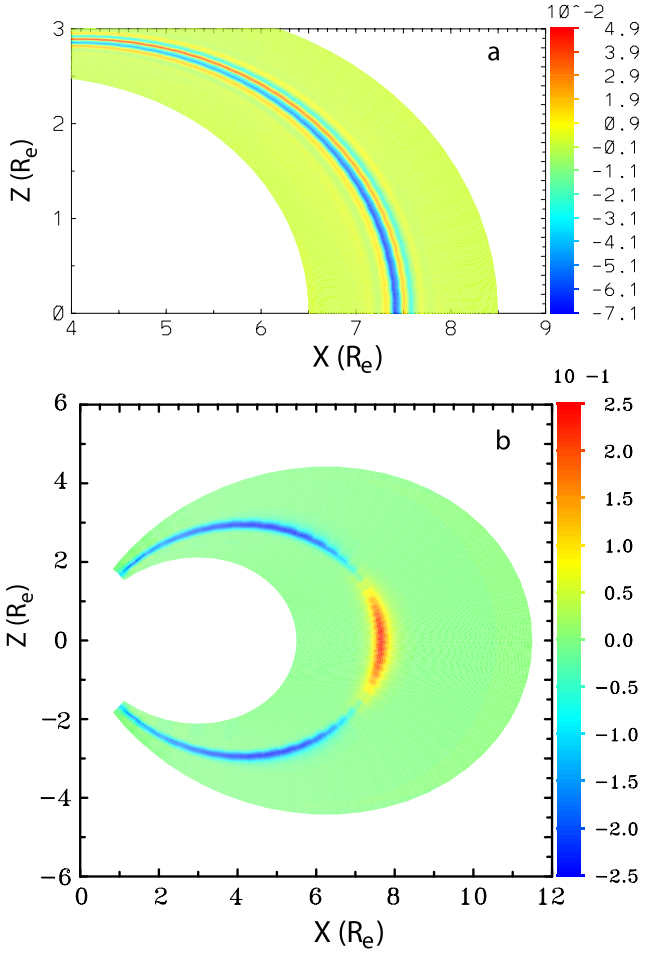

Figure 6. Spatial distribution of the relative density perturbation $\delta\rho/\rho_0$: (a) for the instability case in Figure 1 at $t = 400$ s and (b) for a typical driven FLR at t = 10 periods.

These results are important in the identification of the mechanisms whether an observed ULF geomagnetic pulsation is caused by a FLR or the ionospheric feedback instability if density distribution is known from satellite data.

[22] It is worth noting that the localized electromagnetic waves were usually observed inside the large-scale and broad density cavities [*Staciewicz et al.*, 1998; *Mishin et al.*, 2003; *Chaston et al.*, 2006]. The nonlinear FLR model successfully produces the density cavities with sufficient depth and width together with reasonable wavefields to account for observations [*Lu et al.*, 2003b]. However, (1) the observations mentioned above also show that the density profile inside the broad cavity is highly variable with many small density enhancement or high frequency fluctuations, as pointed out early by *Persoon et al.* [1988]; and (2) FLR theory can not explain the electromagnetic and plasma variations with the same frequency, such as the subauroral wave structure reported by *Mishin et al.* [2003] and *Mishin and Burke* [2005]. The nonlinear feedback instability model provides a natural explanation for the formation of density and electromagnetic perturbations with the same frequency. Short-scale SAWs have high transverse group velocities in the top ionosphere. In FLRs, this

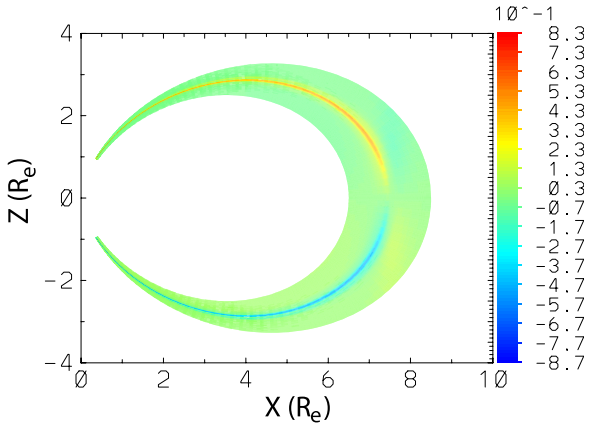

Figure 7. Compressional component b_x due to ponderomotive force at $t = 400$ s for the instability case in Figure 1.

transverse leakage is compensated by the propagation in the opposite direction during the high-β magnetospheric pass. The IAR modes propagate in the low-β plasma and thus must quickly escape the generation region. *Mishin and Förster* [1995] showed that the trapping of small-scale inertial Alfvén waves within a 100 km-scale plasma cavity (transverse waveguide) results in the formation of a quasi-standing wave pattern consisting of a number of paired up/down small-scale FACs, which can explain slow transverse motion of small-scale Alfvén aurora.

[23] Figures 7 and 8 show the b_x and b_z at $t = 400$ s, respectively. Perturbed magnetic fields b_x and b_z associated with the instability both are only ~1 nT, much smaller than the azimuthal magnetic field (over 60 nT).

[24] To investigate the effects of the seasonal conductivity asymmetry, we perform a simulation with different initial Pedersen conductivities between two hemispheres: the minimum initial conductivity in the northern ionosphere is still kept to be 1 mho, representing a low conductivity condition usually observed at nightside and in winter, while the minimum initial conductivity in the southern ionosphere is chosen to be 3 mho for the summer [*Rasmussen et al.*, 1988]. Figure 9 shows the spatial distributions of perpendicular electric field (left) and parallel current density (right) in the computation domain at $t = 300$ s. The top (low)

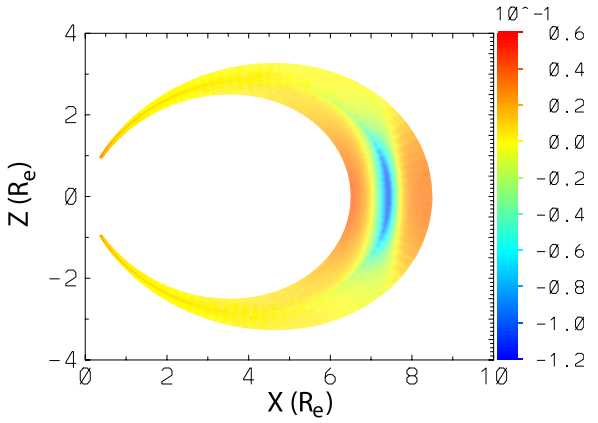

Figure 8. Compressional component b_z due to ponderomotive force at $t = 400$ s for the instability case in Figure 1.

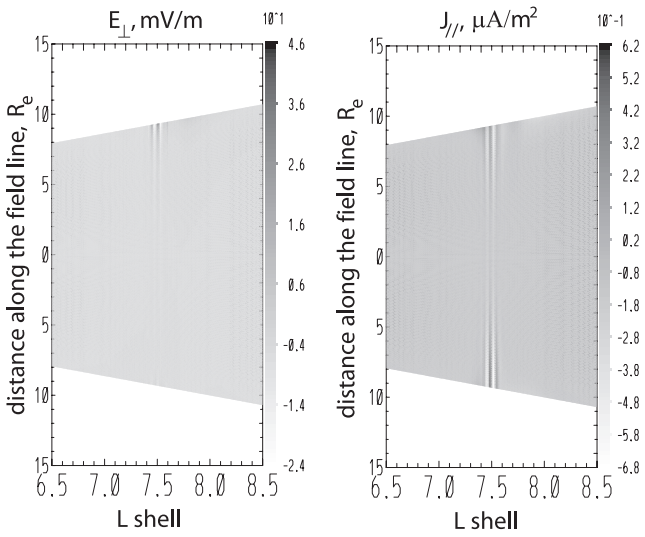

Figure 9. Spatial distributions of perpendicular electric field and parallel current density at $t = 300$ s for seasonal effects of conductivity asymmetry.

boundary of the computation domain is the northern (southern) ionosphere. The perpendicular electric field shows a strong asymmetry between the two hemispheres with much higher amplitude in the northern ionosphere. This result is in agreement with observed conclusions of auroral arcs [*Newell et al.*, 1996, 1998; *Liou et al.*, 1997, 2001].

5. Summary and Conclusions

[25] A newly developed interactive M-I coupling model that describes the dynamic interaction between magnetospheric dispersive waves, compressional modes, and auroral electron precipitations is applied to investigate the geomagnetic ULF pulsations observed in Earth's magnetosphere. The physics based ionospheric ionization model GLOW is incorporated into our 2D finite element code TOPO, making it possible to investigate magnetosphere-ionosphere coupling (through field aligned currents closing by ionospheric cross-field currents) with auroral electron precipitations. The magnetospheric waves are triggered by ionospheric feedback instability from an initially small-scale density perturbation. Two new aspects of this work are that (1) rather than using a linearized approximation, we solve the full nonlinear MHD equations, i.e., we include the full compressional modes and their coupling with dispersive shear Alfvén waves; and (2) we use a more self-consistent, interactive, physics-based ionospheric conductivity model considering the effects of field-aligned potential drops and the magnetic mirror force on electron precipitation.

[26] It is shown that the feedback instability can be triggered by a very small-scale, small amplitude density perturbation (only 1%), and the small-scale wave structures observed by satellites can be attributed to the waves triggered by feedback instability. The auroral electron precipitation can strongly enhance magnetospheric wave amplitudes and density perturbation, and both the ionospheric density perturbation and magnetospheric waves are influenced by the effects that they produce. Precipitating energy and energy flux significantly affect the growing

speed of the feedback instability. Higher precipitation energy and energy flux leads to faster instability growths. However, for lower amplitude FACs, auroral precipitating electrons have no significant effect in feeding back the magnetospheric waves.

[27] The plasma movements in the feedback instability case are very different from that associated with FLRs. In an instability, across the field lines at the equatorial plane, there is plasma moving earthward and anti-earthward; while in FLR, the plasma mainly moves along the field line from high to low latitude (at least for low β plasma). As a result, density redistributions are different between FLRs and the instabilities: In FLR, the plasma mainly moves along the field lines, especially on the resonance shell, resulting in a density bump at the equator and a cavity in the high latitudes close to the ionosphere; while in the feedback instabilities, density is distributed either as bump or cavity along the field line, and across the field lines, cavity and bump occur alternately. We demonstrate that the very large scale and large amplitude cavity across the field line is more possibly generated by FLRs and the higher frequency density fluctuation can be attributed to the feedback instability. These results are important in the identification of the mechanisms and the nonlinear feedback instability model provides a natural explanation for the formation of density and electromagnetic perturbations with the same frequency which disagree with the FLR scenario.

[28] For typical currents observed ($\sim$few μA/m^2), compressional components v_x and v_z are roughly 10–50 times smaller than the azimuthal movement, and perturbed magnetic fields b_x and b_z are also much smaller than the azimuthal magnetic field.

[29] In our calculation, ionospheric Hall current is neglected. Hall current can be ignored if the ion Larmor radius is very small compared to the scale length of the fluid motion. *Nishida* [1978] showed that the role of divergent Hall current can be neglected if the shear Alfvén wave with a low frequency and short horizontal wavelength was incident from the magnetosphere. When the horizontal scale of localized oscillation is of the order of several times of the height of ionosphere, the contribution of the divergent Hall current to the FAC may become important thus possibly affect the coupling between shear and compressional modes [*Ellis and Southwood*, 1983; *Yoshikawa and Itonaga*, 1996]. Therefore a more self-consistent study of M-I coupling needs to include the ionospheric Hall component in the current continuity equation.

[30] Finally, it should be mentioned that this work is limited to small current amplitude systems. For large currents (>10 μA/m^2), the situation could be much more complicated: (1) associated density perturbation could significantly affect the behavior of the plasma; and (2) ionospheric electrons can be heated by shear Alfvén waves through Joule dissipation, which may produce significant ionization and further feedback on the wave amplitude and structure [*Lu et al.*, 2005a, 2005b].

[31] **Acknowledgments.** We are grateful to M. Wiltberger in obtaining electron precipitation from FAC. J. Y. Lu benefited from the discussion with I. Mann. This work was supported in part by the Canadian Space Agency and the Natural Sciences and Engineering Research Council of Canada. This material is also based upon the work supported by CISM which is funded by the STC Program of the National Science Foundation under Agreement Number ATM-0120950. The National Center for Atmospheric Research is sponsored by NSF. Our work made use of the infrastructure and resources of WestGrid.

[32] Amitava Bhattacharjee thanks Evgeny Mishin and another reviewer for their assistance in evaluating this paper.

References

Atkinson, G. (1970), Auroral arcs: Result of the interaction of a dynamic magnetosphere with the ionosphere, *J. Geophys. Res.*, *75*(25), 4746–4755.

Banks, P. M., C. R. Chappell, and A. F. Nagy (1974), A new model for the interaction of auroral electrons with atmosphere: Spectral degradation, backscatter, optical emission, and ionization, *J. Geophys. Res.*, *79*, 1459.

Chaston, C. C., V. Genot, J. W. Bonnell, C. W. Carlson, J. P. McFadden, R. E. Ergun, R. J. Strangeway, E. J. Lund, and K. J. Hwang (2006), Ionospheric erosion by Alfvén waves, *J. Geophys. Res.*, *111*, A03206, doi:10.1029/2005JA011367.

Doe, R. A., M. Mendillo, J. F. Vickrey, L. Z. Zanetti, and R. W. Eastes (1993), Observations of nightside auroral cavities, *J. Geophys. Res.*, *98*(A1), 293–310.

Drozdenko, T., and G. J. Morales (2000), Interaction of a shear Alfvén wave with a filamentary density perturbation in a low-β plasma, *Phys. Plasmas*, *7*, 823.

Ellis, P., and D. J. Southwood (1983), Reflection of Alfvén waves by non-uniform ionospheres, *Planet. Space Sci.*, *31*, 107.

Fridman, M., and J. Lemaire (1980), Relationship between auroral electrons fluxes and field aligned electric potential difference, *J. Geophys. Res.*, *85*(A2), 664–670.

Frycz, P., R. Rankin, J. C. Samson, and V. T. Tikkonchuk (1998), Nonlinear field line resonances: Dispersive effects, *Phys. Plasmas*, *5*, 3565.

Hasegawa, A., and M. M. Wakatani (1983), Finite-larmor-radius magneto-hydrodynamic equations for microturbulence, *Phys. Fluids*, *26*, 2770.

Holzer, T. E., and T. Sato (1973), Quiet auroral arcs and electrodynamic coupling between the ionosphere and magnetosphere, *J. Geophys. Res.*, *78*, 7330.

Knight, S. (1973), Parallel electric fields, *Planet. Space Sci.*, *21*, 741.

Liou, K., P. T. Newell, C.-I. Meng, A. T. Y. Lui, M. Brittnacher, and G. Parks (1997), Synoptic auroral distribution: A survey using Polar ultraviolet imagery, *J. Geophys. Res.*, *102*(A12), 27,197–27,205.

Liou, K., P. T. Newell, and C.-I. Meng (2001), Seasonal effects on auroral particle acceleration and precipitation, *J. Geophys. Res.*, *106*(A4), 5531–5542.

Lu, J. Y., R. Rankin, R. Marchand, and V. T. Tikhonchuk (2003a), Nonlinear acceleration of dispersive effects in field line resonances, *Geophys. Res. Lett.*, *30*(10), 1540, doi:10.1029/2003GL016929.

Lu, J. Y., R. Rankin, R. Marchand, V. T. Tikhonchuk, and J. Wanliss (2003b), Finite element modelling of nonlinear dispersive field line resonances, *J. Geophys. Res.*, *108*(A11), 1394, doi:10.1029/2003JA010035.

Lu, J. Y., R. Rankin, R. Marchand, and V. T. Tikhonchuk (2005a), Nonlinear electron heating by resonant shear Alfvén waves in the ionosphere, *Geophys. Res. Lett.*, *32*, L01106, doi:10.1029/2004GL021830.

Lu, J. Y., R. Rankin, R. Marchand, and V. T. Tikhonchuk (2005b), Reply to comment on "Nonlinear Electron Heating by Resonant Shear Alfvén Waves in the Ionosphere" by J.-P. St.-Maurice, *Geophys. Res. Lett.*, *32*, L13103, doi:10.1029/2005GL023149.

Lu, J. Y., R. Rankin, R. Marchand, I. J. Rae, W. Wang, S. C. Soloman, and J. Lei (2007), Electrodynamics of magnetosphere-ionosphere coupling and feedback on magnetospheric field line resonances, *J. Geophys. Res.*, *112*, A10219, doi:10.1029/2006JA012195.

Lysak, R. L. (1990), Electrodynamic coupling of the magnetosphere and ionosphere, *Space Sci. Rev.*, *53*, 33.

Lysak, R. L. (1991), Feedback instability of the ionospheric resonant cavity, *J. Geophys. Res.*, *96*(A2), 1553–1568.

Lysak, R. L., and Y. Song (2002), Energetics of the ionospheric feedback interaction, *J. Geophys. Res.*, *107*(A8), 1160, doi:10.1029/2001JA000308.

Marchand, R., and M. Simard (1997), Finite element modelling of Tdev edge and divertor with $\mathbf{E} \times \mathbf{B}$ drifts, *Nucl. Fusion*, *37*, 1629.

Mishin, E. V., and M. Banaszkiewicz (1998), On auroral ion conics and electron beams acceleration, *Geophys. Res. Lett.*, *25*(23), 4309, doi:10.1029/1998GL00165.

Mishin, E. V., and W. J. Burke (2005), Stormtime coupling of the ring current, plasmasphere, and topside ionosphere: Electromagnetic and plasma disturbances, *J. Geophys. Res.*, *110*, A07209, doi:10.1029/2005JA011021.

Mishin, E. V., and M. Förster (1995), Alfvénic shocks and low-altitude auroral acceleration, *Geophys. Res. Lett.*, *22*(13), 1745, doi:10.1029/95GL01442.

Mishin, E. V., W. J. Burke, C. Y. Huang, and F. J. Rich (2003), Electromagnetic wave structures within subauroral polarization streams, *J. Geophys. Res.*, *108*(A8), 1309, doi:10.1029/2002JA009793.

Miura, A., and T. Sato (1980), Numerical simulation of global formation of auroral arcs, *J. Geophys. Res.*, *85*(A1), 73–91.

Newell, P. T., C.-I. Meng, and K. M. Lyons (1996), Suppression of discrete aurora by sunlight, *Nature*, *381*, 766.

Newell, P. T., C.-I. Meng, and S. Wing (1998), Relation of solar activity of intense aurorae in sunlight and darkness, *Nature*, *393*, 342.

Nishida, A. (1978), *Geomagnetic Diagnosis of the Magnetospere*, Springer-Verlag, New York.

Nygrén, T., K. U. Kaila, and A. Huuskonen (1992), Determination of E region effective recombination coefficient using impulsive precipitation events, *Geophys. Res. Lett.*, *19*, 445.

Persoon, A. M., D. A. Gurnett, W. K. Peterson, J. H. Waite Jr., J. L. Burch, and J. L. Green (1988), Electron density depletions in the nightside auroral zone, *J. Geophys. Res.*, *93*(A3), 1871–1895.

Pokhotelov, D., W. Lotko, and A. V. Streltsov (2002a), Harmonic structure of field line eigenmodes generated by ionospheric feedback instability, *J. Geophys. Res.*, *107*(A11), 1363, doi:10.1029/2001JA000134.

Pokhotelov, D., W. Lotko, and A. V. Streltsov (2002b), Effects of the seasonal asymmetry in ionospheric Pedersen conductance on the appearance of discrete aurora, *Geophys. Res. Lett.*, *29*(10), 1437, doi:10.1029/2001GL014010.

Pokhotelov, O. A., O. G. Onishchenko, R. Z. Sagdeev, and R. A. Treumann (2003), Nonlinear dynamics of inertial Alfvén waves in the upper ionosphere: Parametric generation of electrostatic convective cells, *J. Geophys. Res.*, *108*(A7), 1291, doi:10.1029/2003JA009888.

Rankin, R., J. C. Samson, V. T. Tikhonchuk, and I. Voronkov (1999), Auroral density fluctuations on dispersive field line resonance, *J. Geophys. Res.*, *104*(A3), 4399–4410.

Rankin, R., K. Kabin, J. Y. Lu, I. R. Mann, R. Marchand, I. J. Rae, V. T. Tikhonchuk, and E. F. Donovan (2005), Magnetospheric field-line resonances: Ground-based observations and modeling, *J. Geophys. Res.*, *110*, A10S09, doi:10.1029/2004JA010919.

Rasmussen, C. E., R. W. Schunk, and V. B. Wickwar (1988), A photochemical equilibrium model for ionospheric conductivity, *J. Geophys. Res.*, *93*(A9), 9831–9840.

Sato, T. (1978), A theory of quiet auroral arcs, *J. Geophys. Res.*, *83*(A3), 1042–1048.

Solomon, S. C., and V. J. Abreu (1989), The 630-nm dayglow, *J. Geophys. Res.*, *94*(A6), 6817–6824.

Solomon, S. C., P. B. Hays, and V. J. Abreu (1988), The auroral 6300 A emission: Observations and modeling, *J. Geophys. Res.*, *93*(A9), 9867–9882.

Song, Y., and R. L. Lysak (2001), Towards a new paradigm: From a quasi-steady description to a dynamical description of the magnetosphere, *Space Sci. Rev.*, *95*, 273.

Staciewicz, K., G. Holmgren, and L. Zanetti (1998), Density depletions and current singularities observed by Freja, *J. Geophys. Res.*, *103*, 4251.

Streltsov, A., and J. C. Foster (2004), Electrodynamics of the magnetosphere-ionosphere couping in the nightside subauroral zone, *Phys. Plasmas*, *11*, 1260, doi:10.1063/1.1647139.

Streltsov, A. V., and W. Lotko (2004), Multiscale electrodynamics of the ionosphere-magnetosphere system, *J. Geophys. Res.*, *109*, A09214, doi:10.1029/2004JA010457.

Streltsov, A. V., and E. V. Mishin (2003), Numerical modeling of localized electromagnetic waves in the nightside subauroral zone, *J. Geophys. Res.*, *108*(A8), 1332, doi:10.1029/2003JA009858.

Streltsov, A., W. Lotko, and G. M. Milikh (2005), Simulation of ULF field-aligned currents generated by HF heating of the ionosphere, *J. Geophys. Res.*, *110*, A04216, doi:10.1029/2004JA010629.

Tikhonchuk, V. T., and R. Rankin (2002), Parallel potential driven by a kinetic Alfvén wave on geomagnetic field lines, *J. Geophys. Res.*, *107*(A7), 1104, doi:10.1029/2001JA000231.

Trakhtengertz, V. Y., and A. Y. Feldstein (1984), Quiet auroral arcs: Ionospheric effect of magnetospheric convection stratification, *Planet. Space Sci.*, *32*, 127.

Trakhtengertz, V. Y., and A. Y. Feldstein (1991), Turbulent Alfvén boundary layer in the polar ionosphere: 1. Excitation conditions and energetics, *J. Geophys. Res.*, *96*, 19,363.

Watanabe, T., H. Oya, K. Watanabe, and T. Sato (1993), Comprehensive simulation study on local and global development of auroral arcs and field-aligned potentials, *J. Geophys. Res.*, *98*(A12), 21,391–21,407.

Wiltberger, M., W. Wang, A. G. Burns, S. C. Solomon, J. G. Lyon, and C. C. Goodrich (2004), Initial results from the coupled magnetosphere-ionosphere-thermosphere model: Magnetospheric and ionospheric responses, *J. Atmos. Solar-Terr. Phys.*, *66*, 1411, doi:10.1016/j.jastp.2004.04.026.

Yoshikawa, A., and M. Itonaga (1996), Reflection of shear Alfvén waves at the ionosphere and the divergent Hall current, *Geophys. Res. Lett.*, *23*(1), 101–104.

G.-M. Le and J.-S. Wang, National Center for Space Weather, China Meteorology Administration, Beijing 100081, China. (wangjs@nsmc.cma.gov.cn)

J. Lei, S. C. Solomon, and W. Wang, High Altitude Observatory, National Center for Atmospheric Research, Boulder, CO 80307, USA. (wbwang@ucar.edu)

J. Y. Lu, R. Marchand, I. J. Rae, and R. Rankin, Department of Physics, University of Alberta, 238 CEB, Edmonton, Alberta, Canada T6G 2G7. (jlu@space.ualberta.ca)